Inorg. Chem. **2006**, *45*, 3665–3670

Synthesis, Structure, and Magnetic Properties of $Cs_{2-x}Rb_xCu_3P_4O_{14}$ ($0.0 \leq x \leq 0.8$): A New Series of Copper(II) Phosphates Containing Periodic Arrays of Staggered Square-Planar CuO_4 Trimers

K. G. Sanjaya Ranmohotti, Xunhua Mo, M. Kirklyn Smith, and Shiou-Jyh Hwu*

Department of Chemistry, Clemson University, Clemson, South Carolina 29634-0973

Received January 13, 2006

In our continued exploratory synthesis of compounds containing transition-metal oxide magnetic nanostructures, a new copper(II) phosphate phase, $Cs_2Cu_3P_4O_{14}$ (**1**), was isolated employing the mixed CsCl/2CsI molten flux. The X-ray single-crystal structural analysis shows that the $Cs_2Cu_3P_4O_{14}$ phase crystallizes in a monoclinic space group with $a = 7.920(2)$ Å, $b = 10.795(2)$ Å, $c = 7.796(2)$ Å, $\beta = 103.90(3)°$, and $V = 646.9(2)$ Å^3; $P2_1/c$ (No. 14); $Z = 2$. The structure has been refined by the full-matrix least-squares method to a final solution with R1 = 0.0248, wR2 = 0.0553, and GOF = 1.02. The three-dimensional Cu–O–P framework exhibits pseudo-one-dimensional channels where the Cs^+ cations reside. The framework consists of trimeric CuO_4 square-planar units stacked in a staggered configuration. These CuO_4 trimers are interlinked by the P_2O_7 units via vertex-sharing O atoms. The stacked CuO_4 units are slanted with respect to the Cu···Cu···Cu vector, resulting in additional Cu–O long bonds, 2.71(1) Å, and a possibly shortened Cu···Cu distance, 3.38(3) Å. **1** shows limited cation substitution with smaller alkali-metal cations; in fact, only a relatively small concentration of Cs^+ can be substituted by Rb^+ to form $Cs_{2-x}Rb_xCu_3P_4O_{14}$ ($0.0 \leq x \leq 0.8$). The temperature-dependent magnetic susceptibility studies of **1** and its Rb-substituted analogues ($x = 0$, 0.33, 0.50, and 0.80) reveal a weak ferromagnetic transition at $T_c = \sim 14$ K, which evidently is independent of the variation of x. In this paper, we report the synthesis, structure, and properties of the title compounds, as well as its brief comparison with the previously discovered $Li_2Cu_3Si_4O_{12}$ phase, which exhibits fused square-planar CuO_4 trimers.

Introduction

Our continued exploratory synthesis of quaternary A−M−X−O oxides, where A = mono- and divalent electropositive cations, M = transition-metal (TM) cations, and X = Si or P, has been fruitful because of the structure versatility of the mixed MO_n ($n = 4-6$) and XO_4 polyhedra. Several newly isolated compounds containing low-dimensional TM oxide lattices form interesting magnetic insulators. Their structures contain periodic arrays of TM oxide magnetic nanostructures that are structurally and electronically confined by the closed-shell, nonmagnetic silicate and phosphate oxyanions. It has been evident that these TM oxide nanostructures form clusters, chains, and layers that frequently mimic the structural unit of some bulk oxides of technological importance.[1] These include, for instance, (1) $La_4Ti(Si_2O_7)_2(TiO_2)_{4m}$ containing single ($m = 1$) and double ($m = 2$) sheets of mixed-valent rutile $[(Ti^{III/IV}O_2)_{4m}]^{4-}$ slabs[2] and (2) $(Ba_3Nb_6Si_4O_{26})_n(Ba_3Nb_8O_{21})$ ($n = 1-4$) possessing slabs of the ReO_3-type mixed-valent $Nb^{IV/V}$ columns.[3] There are also other examples characterized by nanostructures of spin sheet $NaMnAsO_4$, spin chain β-$NaCuPO_4$,[4] $Ba_2Cu(PO_4)_2$,[5] spin tetramers Cu_2PO_4,[6] $Na_5ACu_4(AsO_4)_4Cl_2$ (A = Rb, Cs),[7]

* To whom correspondence should be addressed. E-mail: shwu@clemson.edu.

(1) Hwu, S.-J. *Chem. Mater.* **1998**, *10*, 2846−2859.

(2) (a) Wang, S.; Hwu, S.-J. *J. Am. Chem. Soc.* **1992**, *114*, 6920−6922. (b) Wang, S.; Hwu, S.-J. *Inorg. Chem.* **1995**, *34*, 166−171. (c) Wang, S.; Hwu, S.-J.; Paradis, J. A.; Whangbo, M.-H. *J. Am. Chem. Soc.* **1995**, *117*, 5515−5522. (d) Wang, S. Ph.D. Dissertation, Rice University, Houston, TX, 1993.

(3) (a) Serra, D. L.; Hwu, S.-J. *J. Solid State Chem.* **1992**, *101*, 32−41. (b) Serra, D. L. Ph.D. Dissertation, Rice University, Houston, TX, 1993.

(4) Ulutagay-Kartin, M.; Etheredge, K. M. S.; Schimek, G. L.; Hwu, S.-J. *J. Alloys Compd.* **2002**, *338*, 80−86.

(5) Etheredge, K. M. S.; Hwu, S.-J. *Inorg. Chem.* **1996**, *35*, 1474−1477.

(6) (a) Etheredge, K. M. S.; Hwu, S.-J. *Inorg. Chem.* **1995**, *34*, 5013−5016. (b) Hase, M.; Etheredge, K. M. S.; Hwu, S.-J.; Hirota, K.; Shirane, G. *Phys. Rev. B* **1997**, *56*, 3231−3238. (c) Etheredge, K. M. S. Ph.D. Dissertation, Rice University, Houston, TX, 1996.

10.1021/ic060069t CCC: $33.50
Published on Web 04/06/2006

Scheme 1

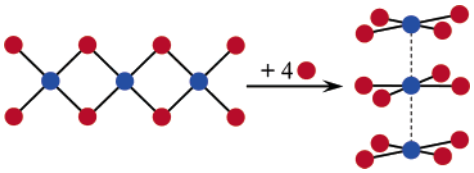

$NaCuAsO_4$,[8] and spin trimers $A_2Cu_3X_4O_{12}$ (A/X = Li/Si, Na/Ge).[6c,9] In theory, these nanostructures could provide a useful model for experimental and theoretical developments of magnetic and electronic interactions in TM oxides because of their simplified structures.[10]

This class of compounds also could be of special interest to the study of new quantum magnetic solids that are complementary to the so-called single-molecule magnets[11] and molecular nanomagnets with respect to the confined magnetic nanostructures.[12] These molecular solids contain soft organic ligands electronically insulating the nanostructures. It should be noted that the development of the molecular magnets has been hampered by their low T_c (<5 K), partially attributed to soft organic components.[13] It was thought that substitution with relatively more rigid inorganic ligands, such as $P_2O_7^{4-}$ anions, could help raise T_c because of reduced phonon interactions.

For the ultimate investigation of theoretical and experimental models of magnetic coupling, we have continued to explore new chemical systems to expand the database of magnetic nanostructures of different size, shape, and geometry. Through molten salt synthesis, we have been able to grow sizable single crystals for structure and property correlation studies. In this paper, we report another fascinating cuprate phosphate $Cs_2Cu_3P_4O_{14}$ (**1**) and its Rb-substituted $Cs_{2-x}Rb_xCu_3P_4O_{14}$ ($x = 0.0-0.8$) analogues.

It is interesting to note that **1** contains spin trimers that can be related to those observed in the $A_2Cu_3X_4O_{12}$ (A/X = Li/Si, Na/Ge) cuprates.[6c] As shown in Scheme 1 (Cu, blue circles; O, red circles), the $[Cu_3O_8]^{10-}$ trimer (left) observed in the $Li_2Cu_3Si_4O_{12}$ framework, for instance, consists of three coplanar CuO_4 units sharing trans edges in a linear fashion. The stacked trimers are interlinked by the parallel $[SiO_3]_\infty$ metasilicate chains to form a ladderlike structure. The $[Cu_3O_{12}]^{18-}$ trimer found in **1** possesses three separated CuO_4 units instead, and they are interlinked by P_2O_7 (not shown) to form the staggered structure (right); see further discussions below. With respect to structure condensation from $[Cu_3O_{12}]^{18-}$ to $[Cu_3O_8]^{10-}$, the formation of a fused trimer in the latter can be considered as the result of a theoretical substitution of the pentavalent P^{5+} cations with the tetravalent Si^{4+} cations. It results in a rather close Cu···Cu distance, 2.96 Å, through the shared O···O edge.[9]

The title compound exhibits a channel-like structure where the Cs^+ cations reside. In an attempt to study the size effect of the monovalent cation to the bulk magnetic properties, we have successively prepared the Rb^+-substituted analogues and examined their magnetic properties systematically. In this report, we discuss the synthesis, structure, and magnetic properties of this new family of copper(II) phosphates, $Cs_{2-x}Rb_xCu_3P_4O_{14}$ ($0.0 \le x \le 0.8$).

Experimental Section

Synthesis. Crystals of $Cs_2Cu_3P_4O_{14}$ (**1**) were grown by employing a molten salt reaction in a fused-silica ampule under vacuum. CuO (7.0 mmol, 99.999%, Strem), P_2O_5 (4.0 mmol, 98+%, Aldrich), CsCl (4.0 mmol, 99.9%, Strem), and CsI (8.0 mmol, 99.9%, Cerac) were mixed and ground in a nitrogen-blanketed drybox. The reaction mixture was then sealed in an evacuated silica tube. The reaction mixture was heated to 700 °C at 1 °C min^{-1}, isothermed for 2 days, and then slowly cooled to 300 °C at 0.1 °C min^{-1} followed by furnace cooling to room temperature. The crystalline phase was retrieved from the flux by washing the product with deionized water using a suction-filtration method. Transparent, blue, column-shaped crystals were isolated. The chemical contents was confirmed by qualitative energy-dispersive X-ray analysis and stoichiometric synthesis.

1 can also be prepared in the polycrystalline form in air using stoichiometric amounts of the corresponding hydroxides and phosphates. For instance, $(NH_4)H_2PO_4$ (7.3 mmol, 99%, Mallinckrodt), $CsOH{\cdot}H_2O$ (3.7 mmol, 99.5%, Acros), and $Cu(OH)_2$ (5.5 mmol, 94%, Alfa) were ground with a limited amount of water (for proper mixing) to allow drying and pressed into a pellet. The reaction mixture was heated to 300 °C at 2 °C min^{-1}, isothermed for 1 day followed by heating to 700 °C at 1 °C min^{-1}, kept at that temperature for 1 day, and finally furnace-cooled to room temperature. Homogeneous, light-blue materials were isolated. The observed powder X-ray diffraction (PXRD) patterns match closely with the one acquired from the single-crystal X-ray diffraction studies (see Figures S1 and S2 in the Supporting Information). The Rb^+-substituted $Cs_{2-x}Rb_xCu_3P_4O_{14}$ ($x = 0$, 0.33, 0.50, and 0.80) was also prepared.[14] Their PXRD data were collected, and refined cell parameters (Table 1) were included for comparison.

Crystallographic Studies. Dark-blue column crystals were physically examined and selected under an optical microscope equipped with a polarizing light attachment. The data crystal was

(7) (a) Hwu, S.-J.; Ulutagay-Kartin, M.; Clayhold, J. A.; Mackay, R.; Wardojo, T. A.; O'Connor, C. J.; Krawiec, M. *J. Am. Chem. Soc.* **2002**, *124*, 12404−12405. (b) Clayhold, J. A.; Ulutagay-Kartin, M.; Hwu, S.-J.; Koo, H.-J.; Whangbo, M.-H.; Voigt, A.; Eaiprasertsak, K. *Phys. Rev. B* **2002**, *66*, 052403/1−052403/4. (c) Ulutagay-Kartin, M. Ph.D. Dissertation, Clemson University, Clemson, SC, 2001.
(8) Ulutagay-Kartin, M.; Hwu, S.-J.; Clayhold, J. A. *Inorg. Chem.* **2003**, *42*, 2405−2409.
(9) Mo, X.; Etheredge, K. M. S.; Hwu, S.; Huang, Q. *Inorg. Chem.* **2006**, *45*, 3478−3480.
(10) For example, see: (a) Snyder, J.; Slusky, J. S.; Cava, R. J.; Schiffer, P. *Nature* **2001**, *413*, 48−51. (b) Koo, H. J.; Whangbo, M. H. *Inorg. Chem.* **2000**, *39* (16), 3599−3604. (c) Goodenough, J. B. *Annu. Rev. Mater. Sci.* **1998**, *28*, 1−27. (d) Goodenough, J. B.; Zhou, J. S. *Chem. Mater.* **1998**, *10* (10), 2980−2993. (e) Tressaud, A.; Dance, J.-M. *Struct. Bonding* **1982**, *52*, 87−146.
(11) For example, see: (a) Lecren, L.; Wernsdorfer, W.; Li, Y.-G.; Roubeau, O.; Miyasaka, H.; Clerac, R. *J. Am. Chem. Soc.* **2005**, *127* (32), 11311−11317. (b) Rajaraman, G.; Murugesu, M.; Sañudo, E. C.; Soler, M.; Wernsdorfer, M.; Helliwell, M.; Muryn, C.; Raftery, J.; Teat, S. J.; Christou, G.; Brechin, E. K. *J. Am. Chem. Soc.* **2004**, *126*, 15445−15447. (c) Wernsdorfer, W.; Aliaga-Alcaldeb, N.; Tirona, R.; Hendricksonc, D. N.; Christou, G. *J. Magn. Magn. Mater.* **2004**, *272*−*276*, 1037−1041.
(12) Thompson, L. K.; Waldmann, O.; Xu, Z. *Coord. Chem. Rev.* **2005**, *249*, 2677−2690.
(13) Ritter, S. K. *Chem. Eng. News: Sci. Technol.* **2004**, *82*, 29−32 and references cited therein.

(14) $Cs_{2-x}Rb_xCu_3(P_2O_7)_2$ (where $x = 0.33$, 0.50, and 0.80) was prepared using the exact experimental procedures and conditions for **1** along with a stoichiometric amount of RbOH (99%, Alfa). Homogeneous, light-blue materials were isolated within 3 days using 0.5 wt % of Li_2CO_3 as the mineralizer during the second heating.

Table 1. Indexed Cell Parameters[a] for **1** (SQUID Sample and As-Prepared Powder) and $Cs_{2-x}Rb_xCu_3(P_2O_7)_2$ ($x = 0.33$, 0.50, and 0.80) Analogues

sample	a (Å)	b (Å)	c (Å)	β (deg)	V (Å^3)
SQUID	7.914(1)	10.795(2)	7.794(1)	103.850(9)	646.5(2)
$x = 0$	7.928(1)	10.793(1)	7.788(1)	103.884(7)	646.9(1)
$x = 0.33$	7.902(2)	10.772(3)	7.799(2)	103.88(2)	644.5(3)
$x = 0.50$	7.842(1)	10.687(2)	7.748(1)	103.763(8)	630.7(2)
$x = 0.80$	7.831(1)	10.679(2)	7.735(1)	103.810(9)	628.2(2)

[a] The cell constants are refined in the monoclinic crystal system. The PXRD pattern is indexed by the DICVOL program using diffraction peaks in the range of $5° \le 2\theta \le 65°$.

Table 2. Crystallographic Data for **1**

empirical formula	$Cs_2Cu_3P_4O_{14}$
fw	804.32
space group, Z	$P2_1/c$ (No. 14), 2
T, °C	27
a, Å	7.920(2)
b, Å	10.795(2)
c, Å	7.796(2)
β, deg	103.90(3)
V, Å^3	646.9(2)
μ(Mo Kα), mm^{-1}	11.004
d_{calc}, g cm^{-3}	4.129
data/restraints/param	1213/0/106
final R1, wR2[a] [$I > 2\sigma(I)$], GOF	0.0221/0.0538/1.02

[a] $R1 = \sum||F_o| - |F_c||/\sum|F_o|$; $wR2 = [\sum w(|F_o| - |F_c|)^2/\sum w|F_o|^2]^{1/2}$; $w = 1/[\sigma^2(F_o^2) + (0.0319P)^2 + 2.51P]$, where $P = (F_o^2 + 2F_c^2)/3$.

Table 3. Atomic Coordinates and Equivalent Displacement Parameters for **1**

atom	Wyckoff notation	x	y	z	U_{iso} (Å^2)[a]
Cs	4e	0.74428(4)	0.18594(3)	0.03965(4)	0.0200(1)
Cu(1)	2c	0	1/2	0	0.0123(2)
Cu(2)	4e	0.28205(6)	0.39187(5)	−0.22806(6)	0.0115(1)
P(1)	4e	0.8698(1)	−0.15854(9)	0.1529(1)	0.0089(2)
P(2)	4e	0.6179(1)	−0.04967(9)	0.3372(1)	0.0096(2)
O(1)	4e	0.8456(4)	−0.1021(3)	−0.0278(4)	0.0141(6)
O(2)	4e	0.9035(4)	−0.2978(3)	0.1592(4)	0.0134(6)
O(3)	4e	0.4586(4)	0.0055(3)	0.2137(4)	0.0140(6)
O(4)	4e	0.5770(4)	−0.1253(3)	0.4853(4)	0.0146(6)
O(5)	4e	0.6874(4)	−0.1474(3)	0.2130(4)	0.0143(6)
O(6)	4e	0.0103(4)	−0.0913(3)	0.2867(4)	0.0142(6)
O(7)	4e	0.7614(4)	0.0453(3)	0.3979(4)	0.0141(6)

[a] Equivalent isotropic U defined as one-third of the trace of the orthogonalized U_{ij} tensor.

mounted on a glass fiber with epoxy for the X-ray diffraction study. The data were collected at room temperature on a four-circle Rigaku AFC8 diffractometer equipped with a Mercury CCD area detector, Mo Kα (λ= 0.710 73 Å) radiation, at $T = 300$ K. The structure was solved by direct methods using the *SHELEX-97* program[15] and refined on F^2 by full-matrix least-squares techniques to R1 = 0.0248, wR2 = 0.0553, and GOF = 1.02 for all data. The final Fourier difference synthesis showed minimum and maximum peaks of −0.712 and +0.736 e Å^{-3}. Table 2 reports the crystallographic data of the structure, and Table 3 lists the atomic parameters.

UV−Vis Diffuse-Reflectance Spectroscopy. Figure 1 shows the optical absorption spectrum of **1** acquired from a PC-controlled Shimadzu UV-3101 UV−vis−NIR spectrometer employing the

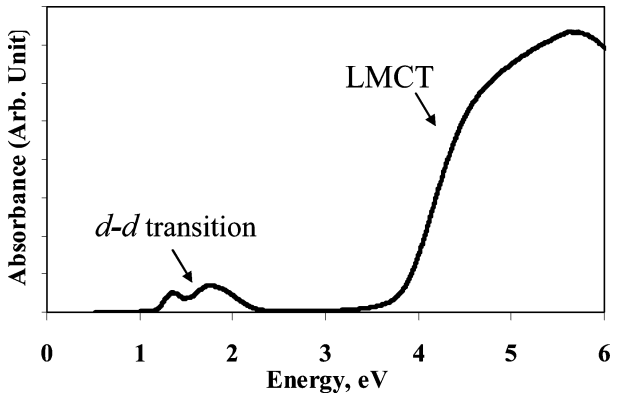

Figure 1. UV−vis diffuse-reflectance spectra of **1**.

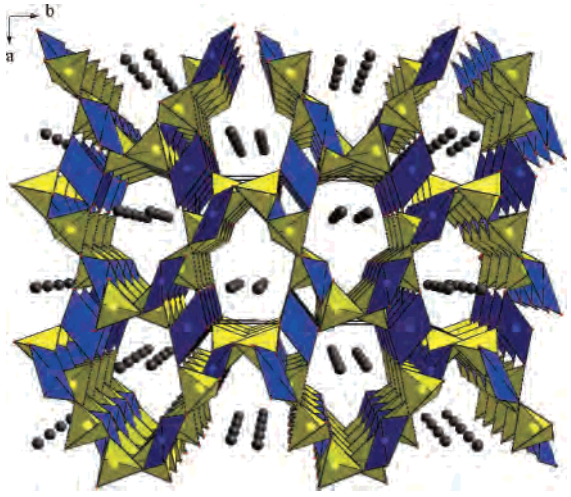

Figure 2. Perspective view of the structure **1** along the *c* axis. The pseudo-one-dimensional channel where the Cs^+ cations (gray, solid circles) reside is made of the edges of the CuO_4 (blue) and PO_4 (yellow) polyhedra.

reported procedures.[16] $BaSO_4$ was used as a reflectance standard. The UV−vis reflectance spectrum was taken in the range of 200 nm (6.2 eV) to 2400 nm (0.50 eV).

Magnetic Susceptibility. Temperature- and field-dependent magnetic measurements of **1** were carried out with a Quantum Design SQUID MPMS-5S magnetometer. The measurements were taken from 2 to 300 K in the applied field of $H = 0.5$ T. Selected crystals of **1** (29.6 mg) were ground and contained in a gel-capsule sample holder. For the Rb^+-substituted compounds, the measurements were carried out on polycrystalline samples. The magnetic susceptibility was corrected for the gel capsule and core diamagnetism with Pascal constants.[17]

Results and Discussion

Figure 2 presents a perspective drawing of the structure **1** viewed along the *c* axis. It shows the pseudo-one-dimensional channel structure where the Cs^+ cations reside. The open framework is made of the Cu−O−P−O−Cu covalent linkages, whereby alternating square-planar [CuO_4] and pyrophosphate [P_2O_7] units share vertex O atoms.

This fascinating three-dimensional framework consists of periodically assembled arrays of $[Cu_3O_{12}]^{18-}$ units that are bridged by the $(P_2O_7)^{4-}$ pyrophosphate anions, as shown in

(15) Sheldrick, G. M. In *Crystallographic Computing 3*; Sheldrick, G. M., Kruger, C., Goddard, R., Eds.; Oxford University Press: London, 1985; pp 175−189. (b) Sheldrick, G. M. In *SHELXTL, Version 6.1, Structure Determination Software Programs*; Bruker Analytical X-ray Systems Inc.: Madison, WI, 2001.

(16) Ulutagay-Kartin, M.; Hwu, S.-J.; Clayhold, J. A. *Inorg. Chem.* **2003**, *42*, 2405−2409.

(17) O'Connor, C. J. *J. Prog. Inorg. Chem.* **1982**, *29*, 203−276.

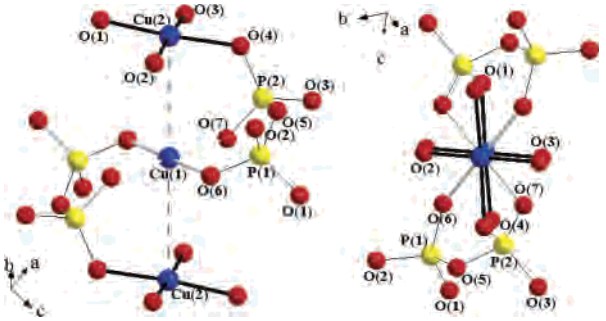

Figure 3. (Left) Side view of stacked square-planar CuO_4 trimeric units interconnected by P_2O_7. The CuO_4 trimer centers around the Cu(1) atom at the center of the inversion symmetry. The Cu−Cu interaction in the trimeric Cu units is indicated by dotted lines. (Right) Top view of the structure showing a staggered configuration. The torsion angles ∠O(*n*)−Cu(1)−Cu(2)−O(*m*), *n*12*m*, are as follows: 43.7(1)°, 6121; 54.7(1)°, 6123; 46.7(1)°, 7123; 36.9(1)°, 7124; 41.6(1)°, 6124; 54.6(2)°, 6122; 46.9(2)°, 7122; 34.7(1)°, 7121.

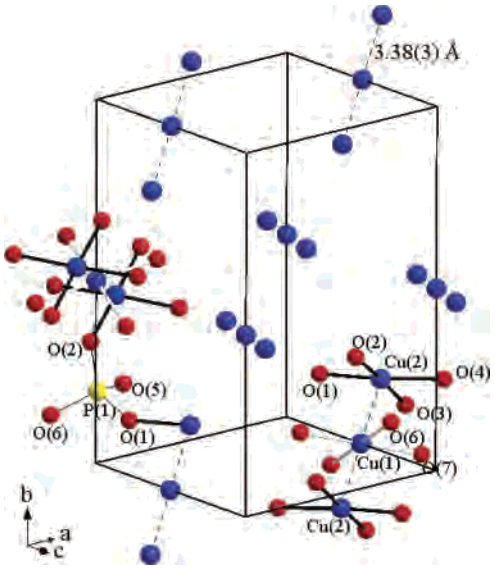

Figure 4. Two sets of symmetry-related Cu−O triplets by the *c*-glide plane interlinked through the $P(1)O_4$ unit. One triplet from each set is completed for clarity. The parallel triplet units are interconnected via $P(2)O_4$ (not shown) of the P_2O_7 pyrophosphate.

Figure 3. The magnetic Cu^{2+} cations reside in the CuO_4 square-planar units. Three CuO_4 units are stacked in a staggered configuration (Figure 3, right), with O−Cu(1)−Cu(2)−O torsion angles ranging from 34.7(1)° to 54.7(1)° as opposed to 45°. The square-planar unit is otherwise flat, in that the Cu atoms lie in the O plane as evidenced by the sum of the ∠O−Cu−O angles, e.g., 360.0(4)° for Cu(1) and 360.3(4)° for Cu(2).

Figure 4 shows that the stacked CuO_4 units are slanted with respect to the Cu(2)···Cu(1)···Cu(2) vector indicated by the nonorthogonal angles, e.g., ca. 66° for Cu(1)−O_4 and 80° for Cu(2)−O_4. The difference in tilting suggests that the two CuO_4 units are not parallel but tilted possibly because of the bond strain of the bridging $P(2)O_4$ unit (Figure 3). The staggered CuO_4 planes, accompanied with the tilting, give rise to additional O coordination to the center Cu with a long Cu(1)−O(2) bond, e.g., 2.71(1) Å, as well as diverse torsion angles mentioned above. Furthermore, the Cu···Cu

Table 4. Selected Bond Distances (Å) for **1**[a]

		$Cu(1)O_6$	
Cu(1)−O(7)^{iii}	1.929(3) (2×)	Cu(1)−O(2)	2.710(3) (2×)
Cu(1)−O(6)^{ii}	1.951(3) (2×)		
		$Cu(2)O_4$	
Cu(2)−O(1)^{i}	1.930(3)	Cu(2)−O(3)^{ii}	1.922(3)
Cu(2)−O(2)^{i}	1.964(3)	Cu(2)−O(4)^{i}	1.961(3)
		$P(1)O_4$	
P(1)−O(1)	1.504(3)	P(1)−O(5)	1.626(3)
P(1)−O(2)	1.525(3)	P(1)−O(6)	1.516(3)
		$P(2)O_4$	
P(2)−O(3)	1.513(3)	P(2)−O(5)	1.616(3)
P(2)−O(4)	1.511(3)	P(2)−O(7)	1.520(3)
		CsO_8	
Cs−O(3)^{i}	3.038(3)	Cs−O(2)^{iii}	3.190(3)
Cs−O(7)^{ii}	3.119(3)	Cs−O(4)^{i}	3.229(3)
Cs−O(7)	3.152(3)	Cs−O(1)^{i}	3.285(3)
Cs−O(6)^{iii}	3.183(3)	Cs−O(1)^{iii}	3.394(3)

[a] Symmetry codes: (i) $-x$, $1.5 + y$, $0.5 - z$; (ii) x, $-1 + y$, z; (iii) $-x$, $2.5 + y$, $0.5 - z$.

distance, 3.38(3) Å, is significantly longer than 2.56 Å, the Cu−Cu distance found in elemental Cu.[18]

As shown in Table 4, the CuO_4 and PO_4 units adopt bond distances normally observed in the copper(II) phosphates.[19] More specifically, the Cu−O bond distances range from 1.92 to 1.96 Å, comparable with 1.92 Å, the sum of the Shannon crystal radii for a four-coordinate Cu^{2+} (0.71 Å) and O^{2-} (1.21 Å).[20] The terminal P−O bond distances, 1.50−1.52 Å, are similar to 1.52 Å, the sum of the Shannon crystal radii for P^{5+} (0.31 Å) and O^{2-} (1.21 Å). As expected, the bridging distances are longer, 1.626(3) Å for P(1)−O(5) and 1.616(3) Å for P(2)−O(5). The bridging angle ∠P(1)−O(5)−P(2) = 132.45(2)° is normal. The corresponding bond valence sum[21] confirms the oxidation states of the Cu^{2+} and P^{5+} cations as 2.09 for Cu(1), 1.95 for Cu(2), 4.92 for P(1), and 4.95 for P(2).

1 forms an interesting spiral $[CuP_2O_7]_\infty$ framework propagating along the 2_1 screw axis, as shown in Figure 5. The spiral structure is formed via vertex-sharing O atoms of square-planar CuO_4 and pyrophosphate P_2O_7 units in an alternating fashion. $Cu(2)O_4$ provides an essential element, allowing the spiral chain to propagate along the 2_1 screw axis, while $Cu(1)O_4$ serves as a linker to interconnect the parallel spiral chains. The flexible $[CuP_2O_7]$ framework revolves around Cs^+ cations, suggesting a templatelike behavior. In addition, the average Cs−O distance is 3.20 Å (Table 3), which is slightly longer than 3.09 Å, the sum of the Shannon crystal radii for an eight-coordinate Cs^+ (1.88 Å) and O^{2-} (1.21 Å). Despite of the long Cs−O distance and channel structure revealed in Figure 2, the compound failed to undergo an ion-exchange reaction in a mixed LiCl (605 °C)/2LiI (449 °C) molten medium at 700 °C.

As portrayed in Figure 6, the temperature dependence of magnetic susceptibility for **1** obeys the ideal Curie−Weiss-

(18) Greenwood, N. N.; Earnshaw, A. *Chemistry of Elements*; Pergamon Press: Oxford, U.K., 1984; p 1366.
(19) Huang, Q.; Ulutagay, M.; Michener, P. A.; Hwu, S.-J. *J. Am. Chem. Soc.* **1999**, *121*, 10323−10326.
(20) Shannon, R. D. *Acta Crystallogr., Sect. A* **1976**, *32*, 751−767.
(21) (a) Brown, I. D.; Altermatt, D. *Acta Crystallogr.* **1985**, *B41*, 244. (b) Brese, N. E.; O'Keefe, M. *Acta Crystallogr.* **1991**, *B47*, 192.

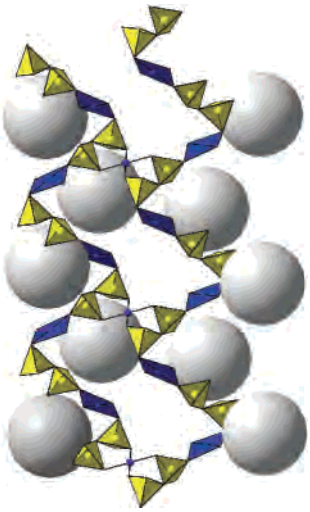

Figure 5. Polyhedral representation showing two parallel $[CuP_2O_7]_\infty$ chains spiral around the 2_1 axis interlinked by, for clarity, one of the $Cu(1)O_4$ units (ball-and-stick drawing; see the text).

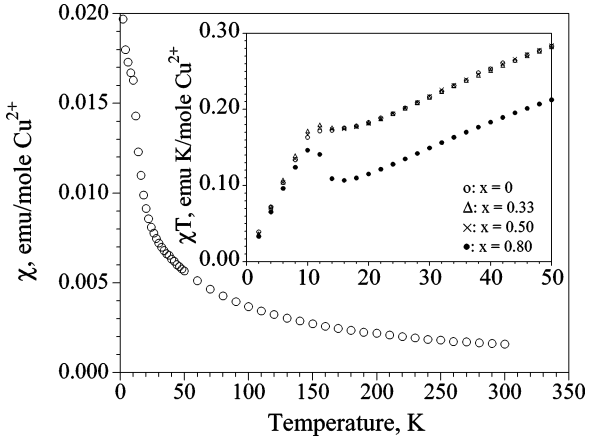

Figure 6. Temperature-dependent magnetic susceptibility of **1**. χT vs T plots of the $Cs_{2-x}Rb_xCu_3P_4O_{14}$ analogues are shown for comparison (inset).

type paramagnetic behavior over the range of 20−300 K along with visible transitions below 20 K. The least-squares fit of the molar magnetic susceptibility data at high temperature to the Curie−Weiss equation, $\chi = \chi_0 + C/(T - \theta)$, where χ_0 is the temperature-independent paramagnetism, C is the Curie constant, θ is the Weiss constant, and T is the temperature, yielded the best-fit values of $\chi_0 = 32(6) \times 10^{-5}$ emu mol^{-1}, $C = 0.43(1)$ emu K mol^{-1}, and $\theta = -31(2)$ K. The calculated μ_{eff} of 1.86(3) μ_B is slightly higher than the ideal value of 1.73 μ_B, a spin-only value for the d^9 Cu^{2+} cation. A negative Weiss constant indicates an antiferromagnetic interaction at high temperature.

1 shows a weak ferromagnetic ordering at $T_c = \sim 14$ K according to the χT vs T plots shown in Figure 6 (inset) from the measurements employing the ground powder from selected crystals. The transition is also obvious in the χ^{-1} vs T plots of the Rb^+-substituted phase, as shown in Figure 7 for the $x = 0.8$ phase (see Figure S3 in the Supporting Information for the plots of all phases). It was noticed that the transition temperature has little dependence on the Rb^+ substitution. Its field-dependent magnetization measurements at 2 K (Figure 7, inset) show a small remnant magnetization

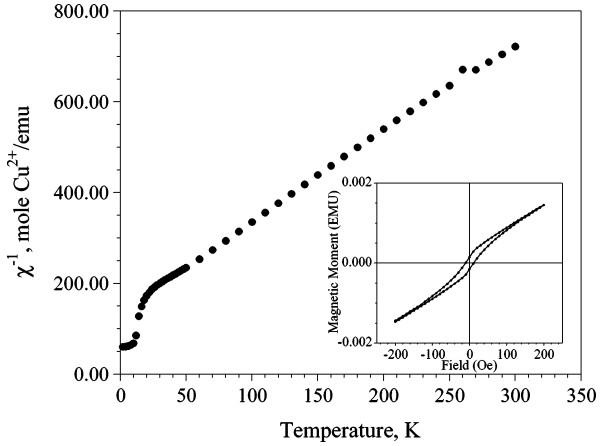

Figure 7. Temperature-dependent magnetic susceptibility of the $Cs_{2-x}Rb_xCu_3P_4O_{14}$, $x = 0.8$, phase. The inset shows the field dependence of the magnetization measured at $T = 2$ K.

and a rather narrow coercive field (<15 Oe). The small hysteresis suggests that this material exhibits soft ferromagnetism. This field-induced ferromagnetic phenomenon is characteristic of low-dimensional metamagnets and can be explained by a canting of the electron spins away from the principal magnetic axis.[4] In the absence of an obvious Cu−O−Cu superexchange pathway, the transition could indicate a mixed antiferro- and ferromagnetism that are due to the Cu−O−P−O−Cu super-superexchange[7b] and the nearly orthogonal ∠Cu(1)−O(2)−Cu(2) = 91.2(2)° through the above-mentioned Cu(1)−O(2) long bond, respectively. The ferromagnetic interaction begins to dominate as the Cu^{2+} magnetic centers are brought closer together because of a decrease in the unit cell volume upon Rb^+ doping (Table 1). It should be noted that a discontinuity observed in both cell volume and χT values (Figure 6, inset) is an intrinsic property, the origin of which needs to be further investigated. In any event, along with the $A_2Cu_3X_4O_{12}$ family, these compounds offer opportunities for the systematic study of spin exchange of magnetic nanostructures of different shape and geometry.

In conclusion, a new cesium−copper(II) phosphate and its Rb^+-substituted analogues $Cs_{2-x}Rb_xCu_3P_4O_{14}$ ($0.0 \le x \le 0.8$) were investigated. The synthesis and crystal growth of **1** were carried out at high temperature employing a mixed CsCl/2CsI molten flux. The structure is characterized by the staggered triple CuO_4 units embedded in a nonmagnetic phosphate oxyanion matrix. Given the weak ferromagnetic coupling and long Cu···Cu intercluster distance (>4.91 Å), this compound series can be viewed as a moleculelike quantum magnetic solid that contains periodic arrays of TM oxide magnetic nanostructures. The high-temperature magnetic data indicate that the Cu−O framework exhibits a spin $^1/_2$ ground state and Curie−Weiss paramagnetic behavior. It shows weak ferromagnetic coupling, and the transition occurs at $T_c = \sim 14$ K independent of the Rb^+ substitution. Nonetheless, the current work in the exploratory synthesis of TM-containing oxy compounds has given a new perspective to the continued investigation of new magnetic insulating materials, and we anticipate more that interesting magne-

tochemistry in this class of compounds containing magnetic nanostructures is yet to come.

Acknowledgment. Financial support for this research (Grants DMR-0077321 and -0322905) and for the purchase of a single-crystal X-ray diffractometer (Grant CHE-9808165) from the National Science Foundation (NSF) is gratefully acknowledged. The authors are indebted to W. Queen for manuscript preparation. M.K.S. especially acknowledges the generous financial support provided via the NSF Summer Research Program in Solid State and Materials Chemistry (Grant DMR-0303450).

Supporting Information Available: X-ray crystallographic file (in CIF format), observed PXRD plots of the $Cs_{2-x}Rb_xCu_3(P_2O_7)_2$ series along with the calculated PXRD of **1**, and temperature-dependent magnetic susceptibility data of **1** and its Rb^+-substitued analogues. This material is available free of charge via the Internet at http://pubs.acs.org.

IC060069T